

# Correlations of net baryon number and electric charge in nuclear matter\*

Xin-ran Yang,<sup>1,2</sup> Guo-yun Shao,<sup>1,2,†</sup> Chong-long Xie,<sup>1,2</sup> and Zhi-Peng Li<sup>1,2</sup>

<sup>1</sup>School of Physics, Xi'an Jiaotong University, Xi'an, 710049, China

<sup>2</sup>MOE Key Laboratory for Nonequilibrium Synthesis and Modulation of Condensed Matter, Xi'an Jiaotong University, Xi'an, 710049, China

We investigate the correlations between net baryon number and electric charge up to sixth order related to the interactions of nuclear matter at low temperature, and explore their relationship with the nuclear liquid-gas phase transition (LGPT) within the framework of the nonlinear Walecka model. The calculation shows that strong correlations between the baryon number and electric charge exist in the vicinity of LGPT, and the higher order correlations are more sensitive than the lower order ones near the phase transition. However, in the high-temperature region away from the LGPT the rescaled lower order correlations are relatively larger than most of the higher order ones. Besides, some of the fifth- and sixth-order correlations possibly change the sign from negative to positive along the chemical freeze-out line with the decrease of temperature. In combination with the future experimental projects at lower collision energies, the derived results can be referred to study the phase structure of strongly interacting matter and analyze the related experimental signals.

Keywords: Correlations of conserved charges, Nuclear matter, Nuclear liquid-gas phase transition, Heavy-ion collision

## I. INTRODUCTION

One of the primary goals in nuclear physics is to map the phase diagram of quantum chromodynamics (QCD). It involves the chiral and deconfinement phase transitions related to the transformation from quark-gluon plasma to hadronic matter [1]. The calculations from lattice QCD and hadron resonance gas (HRG) model indicate that a smooth crossover transformation occurs at high temperature and small chemical potential [2–8]. Moreover, many studies in the effective quark models (e.g., Ref.[9–23]), the Dyson-Schwinger equation approach [24–29], the functional renormalization group theory [30–32] and machine learning [33], suggest that a first-order chiral phase transition undergoes at large chemical potential.

Fluctuations and correlations of conserved charges (baryon number  $B$ , electric charge  $Q$  and strangeness  $S$ ) are sensitive observables to study the phase transition of strongly interacting matter [34, 35]. The net proton (proxy of net baryon) cumulants have been measured in the beam energy scan (BES) program at the Relativistic Heavy Ion Collider (RHIC) [36–42], which has sparked extensive study about QCD phase transition, in particular, the QCD critical endpoint (CEP). More impressively, the distributions of net proton number at the center-of mass energy  $\sqrt{s_{NN}} = 3$  and  $2.4\text{GeV}$  are essentially different from those at  $7.7\text{GeV}$  and above, since the fluctuation distributions of net proton number are primarily dominated by the interaction among

hadrons [40].

The experimental results at  $3\text{GeV}$  and below raise the question of how the hadronic interactions affect the fluctuations of conserved charges at lower-energy regimes [43–46]. With the decrease of collision energy, the nuclear liquid-gas phase transition (LGPT) is possibly involved [47–63]. In Ref. [64–66], a van der Waals model was used to study the high-order distributions of net baryon number in both the pure and mixed phases of the LGPT. In Ref. [45], the second-order susceptibility of net baryon number for positive- and negative-parity nucleons was examined near the chiral and nuclear liquid-gas phase transitions using the double parity model, in which both the chiral phase transition and nuclear LGPT are effectively included. In Ref. [55, 56], the net baryon kurtosis and skewness were considered in the non-linear Walecka model to analyze the experimental signals at lower collision energies. The hyperskewness and hyper-kurtosis of net baryon number were further calculated recently to explore the relation between nuclear LGPT and experimental observables [67].

Since the interactions among hadrons dominate the density fluctuations at lower energy regimes (below  $3\text{GeV}$ ), the BES program at collision energies lower than  $7.7\text{GeV}$  will provide more information about the phase structure of strongly interacting matter. The relevant experiments are also in plan at High Intensity heavy-ion Accelerator Facility (HIAF). Meanwhile, the HADES collaboration at GSI Helmholtzzentrum für Schwerionenforschung planned to measure higher-order net proton and net charge fluctuations in central  $\text{Au} + \text{Au}$  reactions at collision energies ranging from  $0.2A$  to  $1.0A\text{GeV}$  to probe the LGPT region [68]. These experiments are significant for investigating the nuclear liquid-gas and chiral phase transitions through the density fluctuations.

Besides the fluctuations of conserved charges, the correlations of different conserved charges can also provide

\* Supported by the National Natural Science Foundation of China under Grant No. 12475145, 11875213, and the Natural Science Basic Research Plan in Shaanxi Province of China (Program No. 2024JC-YBMS-018)

† Corresponding author, [gyshao@mail.xjtu.edu.cn](mailto:gyshao@mail.xjtu.edu.cn)

67 important information to explore the phase transition.  
 68 The correlations of conserved charges or the off-diagonal  
 69 susceptibilities have been calculated to study the chiral  
 70 and deconfinement phase transitions at high temperature  
 71 in lattice QCD and some effective quark models (e.g.,  
 72 [69–75]). However, the correlations of net baryon num-  
 73 ber and electric charge in nuclear matter and their rela-  
 74 tionship with nuclear LGPT are still absent, which are  
 75 useful in diagnosing the phase diagram of strongly in-  
 76 teracting matter at low temperature. In this study, we  
 77 will explore the correlations between net baryon number  
 78 and electric charge up to sixth order in nuclear matter  
 79 using the nonlinear Walecka model. Some characteristic  
 80 behaviors of correlations evoked by the nucleon-nucleon  
 81 interaction near and far away from the nuclear LGPT  
 82 are obtained. These results will help analyze the chiral  
 83 phase transition, nuclear LGPT and the related experi-  
 84 mental signals in the future.

85 The paper is organized as follows. In Sec. II, we intro-  
 86 duce the formulas to describe correlations of conserved  
 87 charges and the nonlinear Walecka model. In Sec. III,  
 88 we illustrate the numerical results of correlations of net  
 89 baryon number and electric charge. A summary is finally  
 90 given in Sec. IV.

## 91 II. THEORETICAL DESCRIPTIONS

92 The fluctuations and correlations of conserved charges  
 93 are related to the equation of state of a thermodynamic  
 94 system. In the grand-canonical ensemble of strongly in-  
 95 teracting matter the pressure is the logarithm of parti-  
 96 tion function [76]:

$$97 P = \frac{T}{V} \ln Z(V, T, \mu_B, \mu_Q, \mu_S), \quad (1)$$

98 where  $\mu_B, \mu_Q, \mu_S$  are the chemical potentials of con-  
 99 served charges, i.e., the baryon number, electric charge  
 100 and strangeness in strong interaction, respectively. The  
 101 generalized susceptibilities can be derived by taking the  
 102 partial derivatives of the pressure with respect to the  
 103 corresponding chemical potentials [39]

$$104 \chi_{ijk}^{BQS} = \frac{\partial^{i+j+k} [P/T^4]}{\partial(\mu_B/T)^i \partial(\mu_Q/T)^j \partial(\mu_S/T)^k}. \quad (2)$$

105 In experiments, the cumulants of multiplicity distri-  
 106 butions of the conserved charges are usually measured.  
 107 They are related to the generalized susceptibilities by

$$108 C_{ijk}^{BQS} = \frac{\partial^{i+j+k} \ln[Z(V, T, \mu_B, \mu_Q, \mu_S)]}{\partial(\mu_B/T)^i \partial(\mu_Q/T)^j \partial(\mu_S/T)^k} = VT^3 \chi_{ijk}^{BQS}. \quad (3)$$

109 To eliminate the volume dependence in heavy-ion colli-  
 110 sion experiments, observables are usually constructed by  
 111 the ratios of cumulants, and then can be compared with  
 112 the theoretical calculations of the generalized suscepti-  
 113 bilities with

$$114 \frac{C_{ijk}^{BQS}}{C_{lmn}^{BQS}} = \frac{\chi_{ijk}^{BQS}}{\chi_{lmn}^{BQS}}. \quad (4)$$

115 In this research the nonlinear Walecka model is taken  
 116 to calculate the correlations of net baryon number and  
 117 electric charge in nuclear matter at low temperature.  
 118 This model is generally used to describe the properties of  
 119 finite nuclei and the equation of state of nuclear matter.  
 120 The approximate equivalence of this model to the hadron  
 121 resonance gas model at low temperature and small den-  
 122 sity was also indicated in Ref. [77]. This model was re-  
 123 cently taken to explore the fluctuations of net baryon  
 124 number in nuclear matter, e.g., the kurtosis and skew-  
 125 ness in Refs. [55, 56], and the hyperskewness and hyper-  
 126 kurtosis [67].

127 The Lagrangian density for the nucleons-meson system  
 128 in the nonlinear Walecka model [54, 78] is

$$129 \mathcal{L} = \sum_N \bar{\psi}_N [i\gamma_\mu \partial^\mu - (m_N - g_\sigma \sigma) - g_\omega \gamma_\mu \omega^\mu - g_\rho \gamma_\mu \boldsymbol{\tau} \cdot \boldsymbol{\rho}^\mu] \psi_N \\ 130 + \frac{1}{2} (\partial_\mu \sigma \partial^\mu \sigma - m_\sigma^2 \sigma^2) - \frac{1}{3} b m_N (g_\sigma \sigma)^3 - \frac{1}{4} c (g_\sigma \sigma)^4 \\ 131 + \frac{1}{2} m_\omega^2 \omega_\mu \omega^\mu - \frac{1}{4} \omega_{\mu\nu} \omega^{\mu\nu} \\ 132 + \frac{1}{2} m_\rho^2 \boldsymbol{\rho}_\mu \cdot \boldsymbol{\rho}^\mu - \frac{1}{4} \boldsymbol{\rho}_{\mu\nu} \cdot \boldsymbol{\rho}^{\mu\nu}, \quad (5)$$

133 where  $\omega_{\mu\nu} = \partial_\mu \omega_\nu - \partial_\nu \omega_\mu$ ,  $\rho_{\mu\nu} = \partial_\mu \boldsymbol{\rho}_\nu - \partial_\nu \boldsymbol{\rho}_\mu$  and  $m_N$  is  
 134 the nucleon mass in vacuum. The interactions between  
 135 nucleons are mediated by  $\sigma$ ,  $\omega$ ,  $\rho$  mesons..

136 The thermodynamic potential can be derived in the  
 137 mean-field approximation

$$138 \Omega = -\beta^{-1} \sum_N 2 \int \frac{d^3 \mathbf{k}}{(2\pi)^3} \left[ \ln \left( 1 + e^{-\beta(E_N^*(\mathbf{k}) - \mu_N^*)} \right) \right. \\ 139 \left. + \ln \left( 1 + e^{-\beta(E_N^*(\mathbf{k}) + \mu_N^*)} \right) \right] + \frac{1}{2} m_\sigma^2 \sigma^2 + \frac{1}{3} b m_N (g_\sigma \sigma)^3 \\ 140 + \frac{1}{4} c (g_\sigma \sigma)^4 - \frac{1}{2} m_\omega^2 \omega^2 - \frac{1}{2} m_\rho^2 \rho_3^2, \quad (6)$$

141 where  $\beta = 1/T$ ,  $E_N^* = \sqrt{k^2 + m_N^{*2}}$ , and  $\rho_3$  is the third  
 142 component of  $\rho$  meson field. The effective nucleon mass  
 143  $m_N^* = m_N - g_\sigma \sigma$  and the effective chemical potential  $\mu_N^*$   
 144 is defined as  $\mu_N^* = \mu_N - g_\omega \omega - \tau_{3N} g_\rho \rho_3$  ( $\tau_{3N} = 1/2$  for  
 145 proton,  $-1/2$  for neutron).

146 By minimizing the thermodynamical potential

$$147 \frac{\partial \Omega}{\partial \sigma} = \frac{\partial \Omega}{\partial \omega} = \frac{\partial \Omega}{\partial \rho_3} = 0, \quad (7)$$

148 the meson field equations can be derived as

$$149 g_\sigma \sigma = \left( \frac{g_\sigma}{m_\sigma} \right)^2 \left[ \rho_p^s + \rho_n^s - b m_N (g_\sigma \sigma)^2 - c (g_\sigma \sigma)^3 \right], \quad (8)$$

$$151 g_\omega \omega = \left( \frac{g_\omega}{m_\omega} \right)^2 (\rho_p + \rho_n), \quad (9)$$

152

$$153 \quad g_\rho \rho_3 = \frac{1}{2} \left( \frac{g_\rho}{m_\rho} \right)^2 (\rho_p - \rho_n). \quad (10)$$

154 In Eqs.(8)-(10), the nucleon number density

$$155 \quad \rho_i = 2 \int \frac{d^3 k}{(2\pi)^3} [f(E_i^* - \mu_i^*) - \bar{f}(E_i^* + \mu_i^*)], \quad (11)$$

156 and the scalar density

$$157 \quad \rho_i^s = 2 \int \frac{d^3 k}{(2\pi)^3} \frac{m_i^*}{E_i^*} [f(E_i^* - \mu_i^*) + \bar{f}(E_i^* + \mu_i^*)], \quad (12)$$

158 where  $f(E_i^* - \mu_i^*)$  and  $\bar{f}(E_i^* + \mu_i^*)$  are the fermion and  
159 antifermion distribution functions with

$$160 \quad f(E_i^* - \mu_i^*) = \frac{1}{1 + \exp \{[E_i^* - \mu_i^*] / T\}}, \quad (13)$$

161 and

$$162 \quad f(E_i^* + \mu_i^*) = \frac{1}{1 + \exp \{[E_i^* + \mu_i^*] / T\}}. \quad (14)$$

163 The meson field equations can be solved for a given  
164 temperature and chemical potential (or baryon number  
165 density). The model parameters,  $g_\sigma, g_\omega, g_\rho, b$  and  $c$ , are  
166 listed in Table 1. They are fitted with the compression  
167 modulus  $K = 240$  MeV, the symmetric energy  $a_{sym} =$   
168  $31.3$  MeV, the effective nucleon mass  $m_N^* = m_N - g_\sigma \sigma =$   
169  $0.75 m_N$  and the binding energy  $B/A = -16.0$  MeV at  
170 nuclear saturation density with  $\rho_0 = 0.16$  fm $^{-3}$ .

TABLE 1. Parameters in the nonlinear Walecka model

$(g_\sigma/m_\sigma)^2/\text{fm}^2$	$(g_\omega/m_\omega)^2/\text{fm}^2$	$(g_\rho/m_\rho)^2/\text{fm}^2$	$b$	$c$
10.329	5.423	0.95	0.00692	-0.0048

171

172

### III. RESULTS AND DISCUSSION

174 In this section, we present the numerical results of  
175 the correlations between net baryon number and electric  
176 charge in the non-linear Walecka model. To simulate the  
177 physical conditions in the BES program at RHIC STAR,  
178 the isospin asymmetric nuclear matter is considered in  
179 the calculation with the constraint of  $\rho_Q/\rho_B = 0.4$ . In  
180 the present Walecka model, strange baryons are not in-  
181 cluded, thus the strangeness condition of  $\rho_S = 0$  is au-  
182 tomatically satisfied. Note that  $\rho_Q/\rho_B = 0.4$  might be  
183 slightly deviated due to isospin dynamics. We will de-  
184 tailedly explore the influence of different isospin asym-  
185 metries on the fluctuations and correlations of conserved  
186 charges in a separate study.

187 The correlations between baryon number and electric  
188 charge are related to the baryon chemical potential  $\mu_B$   
189 and isospin chemical potential  $\mu_Q$  ( $\mu_Q = \mu_p - \mu_n$ ). To

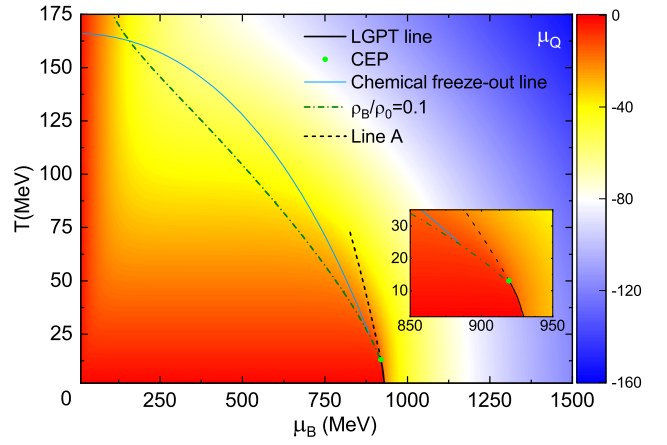


Fig. 1. Contour of  $\mu_Q$  in the  $T - \mu_B$  plane derived in the nonlinear Walecka model with the constraint of  $\rho_Q/\rho_B = 0.4$ . The solid line is the liquid-gas transition line with a CEP locating at  $T = 13$  MeV and  $\mu_B = 919$  MeV. The blue line is the chemical freeze-out line fitted in Ref. [79]. The dash-dotted line corresponds to the temperature and chemical potential for  $\rho_B = 0.1\rho_0$ . “Line A” is derived with  $\partial\sigma/\partial\mu_B$  taking the maximum value for each given temperature.

190 demonstrate the value of  $\mu_Q$  as a function of temperature  
191 and baryon chemical potential, we first plot in Fig. 1 the  
192 contour map of  $\mu_Q$  in the  $T - \mu_B$  plane derived under the  
193 constraint of  $\rho_Q/\rho_B = 0.4$ . The corresponding liquid-gas  
194 phase transition line with a CEP locating at  $T = 13$  MeV  
195 and  $\mu_B = 919$  MeV is also plotted in this figure. To  
196 compare with the chiral crossover phase transition of  
197 quarks, the dashed line labeled as “Line A” in Fig. 1 is  
198 derived with the condition that  $\partial\sigma/\partial\mu_B$  takes the maxi-  
199 mum value for each given temperature. This line plays a  
200 role analogous in a certain degree to the chiral crossover  
201 transformation, although it is not a true phase transi-  
202 tion in nuclear matter. It indicates the location where  
203 the dynamical nucleon mass changes most quickly with  
204 the increase of chemical potential. The reason for this is  
205 to emphasize that both the  $\sigma$  field in nuclear matter and  
206 quark condensate in quark matter are associated with  
207 the dynamical mass of fermions and, therefore the rapid  
208 change of mass might have the universal effect on fluctu-  
209 ation distributions of conserved charges. As pointed out  
210 in our previous studies [54, 55, 67], the location of line  
211 A helps understand the behaviors of interaction mea-  
212 surement (trace anomaly), the fluctuations of conserved  
213 charges near the phase transition [55, 67].

214 One can also define “Line A” by the maximum point of  
215  $\partial\omega/\partial\mu_B$  or  $\partial n_B/\partial\mu_B$ , since the density can be taken as  
216 the order parameter for liquid-gas phase transition. Un-  
217 der this definition, the result obtained in quark model  
218 does not correspond to the chiral crossover phase transi-  
219 tion. This is not the purpose of this study. Our aim is  
220 to indicate some common properties related to dynamical  
221 fermion mass near the critical region of a first-order

222 phase transition. On the other hand, the calculation in  
 223 dicates that the curves (“Line A”) under the two defini-  
 224 tions coincide near the critical region, and the two curves  
 225 gradually deviate at higher temperatures away from the  
 226 critical region.

227 For the convenience of subsequent discussion of exper-  
 228 imental observables, we also plot in Fig. 1 the chemical  
 229 freeze-out line fitted with experimental data at high en-  
 230 ergies [79], which can be described with

$$231 \quad T(\mu_B) = a - b\mu_B^2 - c\mu_B^4, \quad (15)$$

232 where  $a = 0.166 \text{ GeV}$ ,  $b = 0.139 \text{ GeV}^{-1}$  and  $c =$   
 233  $0.053 \text{ GeV}^{-3}$ . We should remind that the trajectories of  
 234 the present relativistic heavy-ion collisions do not pass  
 235 through the  $T_C$  of nuclear LGPT. It is still not known  
 236 how far the realistic chemical freeze-out line is from the  
 237 critical region in future experiments. However, similar  
 238 to the chiral phase transition of quarks, the existence of  
 239 nuclear LGPT affects the fluctuation and correlation of  
 240 net baryon and electric charge number in the region not  
 241 very adjacent to the critical end point in intermediate-  
 242 energy heavy-ion collision experiments. The numerical  
 243 results on the parameterized chemical freeze-out line in  
 244 this study can be taken as a reference. The realistic  
 245 chemical freeze-out condition at intermediate and low  
 246 energies will be extracted in future heavy-ion collision  
 247 experiments. When analyzing the experimental data the  
 248 contribution from LGPT needs to be considered.

249 Fig. 1 shows that the value of  $|\mu_Q|$  is smaller than  
 250  $40 \text{ MeV}$  in the area covered in red. In this region the  
 251 baryon number density is very small, which can be seen  
 252 roughly from the temperature and chemical potential  
 253 curve for  $\rho_B = 0.1\rho_0$  (dash-dotted line). The value  
 254 of  $|\mu_Q|$  increases with the rising baryon density (cor-  
 255 sponding to larger chemical potential). This trend of  
 256  $|\mu_Q|$  is clearly illustrated in Fig. 1. Along the chemi-  
 257 cal freeze-out line (solid blue line), one can see how  $\mu_Q$   
 258 changes at freeze-out with the decrease of temperature  
 259 or collision energy.

260 We demonstrate in Fig. 2 the second order cor-  
 261 relation between baryon number and electric charge,  
 262  $\chi_{11}^{BQ}/\chi_2^Q$ , as functions of baryon chemical potential for  
 263  $T = 75, 50, 25 \text{ MeV}$ , respectively. To derive the phys-  
 264 ical quantity comparable with future experiments the  
 265 correlated susceptibility is divided by  $\chi_2^Q$ , which elimi-  
 266 nates the volume dependence. For each temperature, the  
 267 rescaled second-order correlation  $\chi_{11}^{BQ}/\chi_2^Q$  in Fig. 2 dis-  
 268 plays a nonmonotonic behavior with a peak structure at  
 269 a certain chemical potential. The values of these peaks  
 270 increase with the decline of temperature, which indi-  
 271 cate the correlation between baryon number and electric  
 272 charge is enhanced near the phase transition region. The  
 273 solid dots in Fig. 2 demonstrate the values at chemical  
 274 freeze-out described by Eq. (15), which illustrate that  
 275 the value of  $\chi_{11}^{BQ}/\chi_2^Q$  increases along the freeze-out line  
 276 when moving from the high-temperature side to the crit-  
 277 ical region.

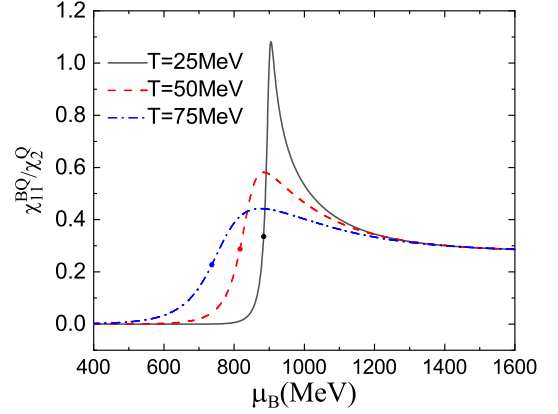


Fig. 2. Second order correlation between baryon number and electric charge as a function of chemical potential for different temperatures. The solid dots demonstrate the values on the chemical freeze-out line given in Fig. 1.

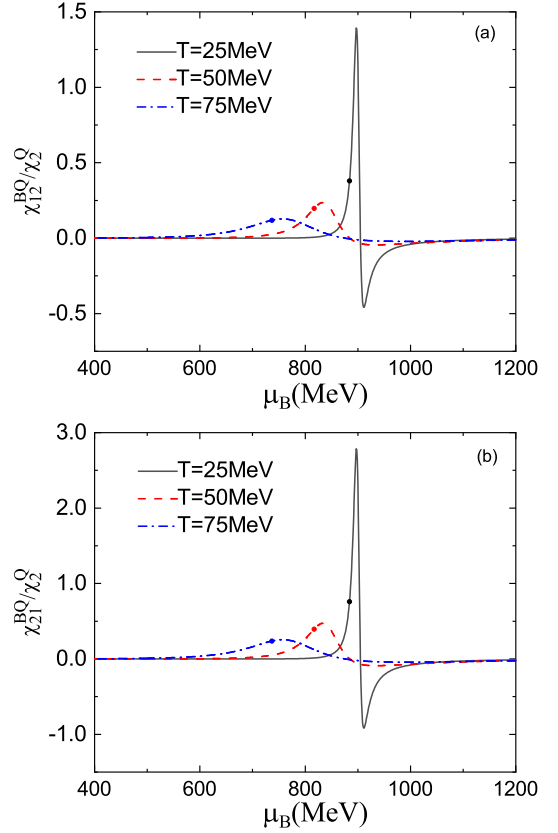


Fig. 3. Third order correlations between baryon number and electric charge as functions of chemical potential at different temperatures. The solid dots demonstrate the values on the chemical freeze-out line plotted in Fig. 1.

Fig. 3 shows the third order correlations,  $\chi_{12}^{BQ}/\chi_2^Q$  and  $\chi_{21}^{BQ}/\chi_2^Q$ , as functions of chemical potential for several temperatures. Compared with the  $\chi_{12}^{BQ}/\chi_2^Q$ , the fluctuation of  $\chi_{21}^{BQ}/\chi_2^Q$  is relatively larger at the same temperature. The solid dots at chemical freeze-out line present the same trend. This means the measurement of  $\chi_{21}^{BQ}/\chi_2^Q$  is more sensitive than  $\chi_{12}^{BQ}/\chi_2^Q$  in heavy-ion collision experiments. Fig. 3 also indicates that with the decrease of temperature, the correlations between baryon number and electric charge intensify. An evident oscillations of  $\chi_{12}^{BQ}/\chi_2^Q$  and  $\chi_{21}^{BQ}/\chi_2^Q$  appear for  $T = 25$  MeV, accompanied by the alternating positives and negatives. With the decrease of temperature, the divergent behavior appears at the CEP of LGPT. These features can be used to look for the signal of phase transition in experiments.

In Fig. 4, we plot the fourth order correlations between baryon number and electric charge,  $\chi_{13}^{BQ}/\chi_2^Q$ ,  $\chi_{22}^{BQ}/\chi_2^Q$  and  $\chi_{31}^{BQ}/\chi_2^Q$ . Compared with the second and third order correlations in Fig. 2 and Fig. 3, Fig. 4 shows that the rescaled fourth order correlations by  $\chi_2^Q$  are weaker at higher temperature, e.g.,  $T = 75$  MeV. However, the correlations are much stronger at  $T = 25$  MeV, near the critical region of LGPT. Correspondingly, there is evidently a bimodal structure for all the three correlations with the increase of chemical potential at lower temperature. It is also seen that the maximum values of  $\chi_{13}^{BQ}/\chi_2^Q$ ,  $\chi_{22}^{BQ}/\chi_2^Q$  and  $\chi_{31}^{BQ}/\chi_2^Q$  increase in turn. Besides, the solid dots demonstrate the value of each correlation at freeze-out increases with the decline of temperature. Moreover, it is seen that  $\chi_{13}^{BQ}/\chi_2^Q < \chi_{22}^{BQ}/\chi_2^Q < \chi_{31}^{BQ}/\chi_2^Q$  at chemical freeze-out for each temperature. It implies that  $\chi_{31}^{BQ}/\chi_2^Q$  is most sensitive among the three fourth-order correlations.

Fig. 5 presents the fifth order correlations between baryon number and electric charge,  $\chi_{14}^{BQ}/\chi_2^Q$ ,  $\chi_{23}^{BQ}/\chi_2^Q$ ,  $\chi_{32}^{BQ}/\chi_2^Q$  and  $\chi_{41}^{BQ}/\chi_2^Q$  for  $T = 75, 50, 25$  MeV. This figure shows that at  $T = 75$  MeV, the values of the three rescaled correlations are all quite small, but they become drastic at  $T = 25$  MeV. In combination with the phase diagram in Fig. 1, it can be seen that the closer they get to the liquid-gas transition the stronger the high-order correlated fluctuations. Similar to the fourth order correlations, the rescaled fifth correlations fulfill the relations of  $|\chi_{14}^{BQ}/\chi_2^Q| < |\chi_{23}^{BQ}/\chi_2^Q| < |\chi_{32}^{BQ}/\chi_2^Q| < |\chi_{41}^{BQ}/\chi_2^Q|$  at chemical freeze-out. Moreover, a remarkable result is that all the four fifth-order correlation fluctuations are negative at chemical freeze-out for  $T = 75$  and 50 MeV, but they are positive at  $T = 25$  MeV, close to the region of liquid-gas transition. This is a prominent feature in exploring the interaction and phase transition of nuclear matter.

Fig. 6 shows the sixth order correlations of baryon number and electric charge, i.e.,  $\chi_{15}^{BQ}/\chi_2^Q$ ,  $\chi_{24}^{BQ}/\chi_2^Q$ ,  $\chi_{33}^{BQ}/\chi_2^Q$ ,  $\chi_{42}^{BQ}/\chi_2^Q$  and  $\chi_{51}^{BQ}/\chi_2^Q$ . Each of the sixth order correlations has a double-peak and double-valley

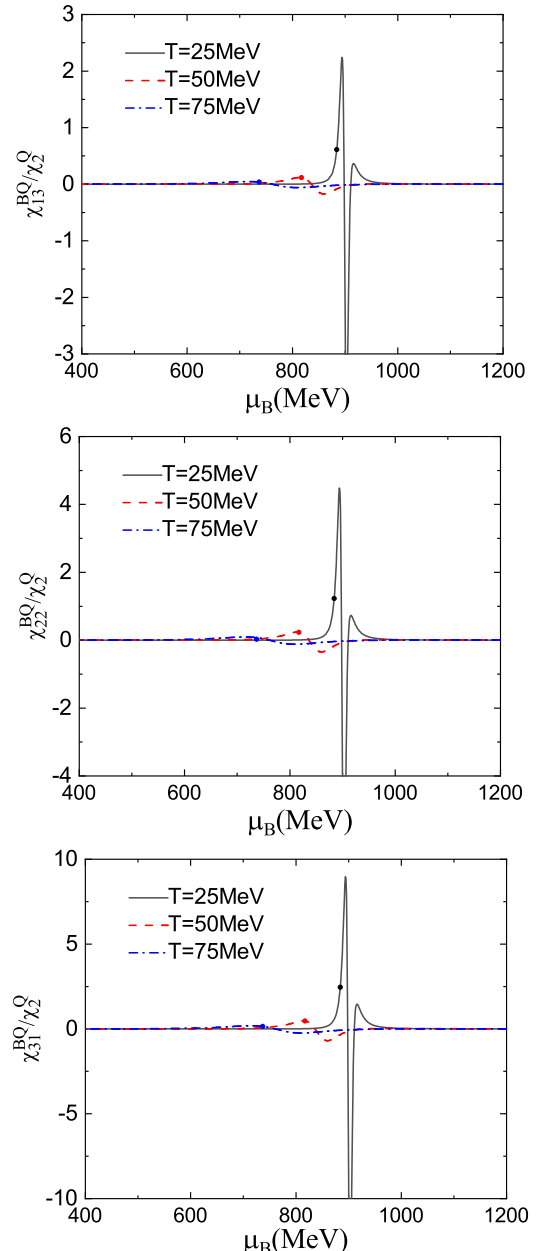


Fig. 4. Fourth order correlations between baryon number and electric charge as functions of chemical potential for different temperatures. The solid dots demonstrate the values on the chemical freeze-out line given in Fig. 1.

structure, although one of the two peaks is not prominent. It is seen that the oscillating behavior intensifies when moving towards the phase transition region from high temperatures to lower ones. Similarly, the intensity of oscillations increases in turn from  $\chi_{15}^{BQ}/\chi_2^Q$ ,  $\chi_{24}^{BQ}/\chi_2^Q$ ,  $\chi_{33}^{BQ}/\chi_2^Q$ ,  $\chi_{42}^{BQ}/\chi_2^Q$  to  $\chi_{51}^{BQ}/\chi_2^Q$ .

For a given order of correlations, the numerical results in Fig. 2-6 show that the signals become stronger when there are more derivatives with respect to baryon

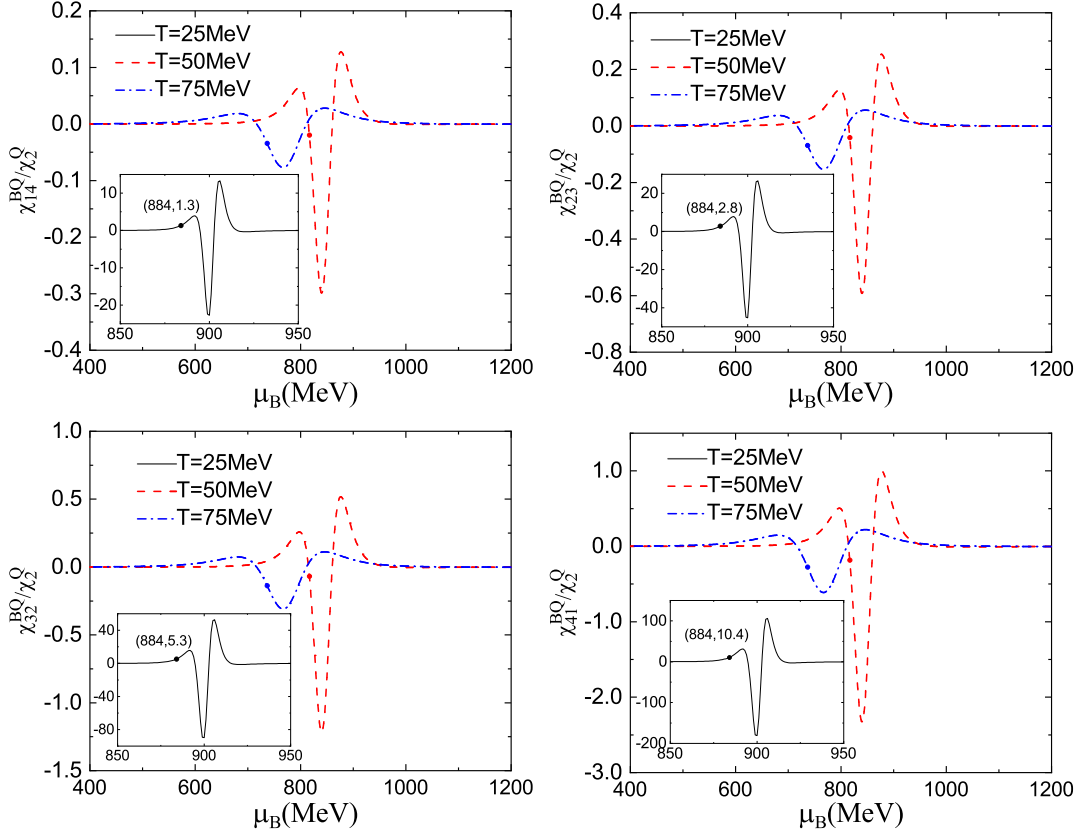


Fig. 5. Fifth order correlations between baryon number and electric charge as functions of chemical potential for different temperatures. The solid dots demonstrate the values on the chemical freeze-out line given in Fig. 1.

chemical potential than that with to electric chemical potential. We also checked the pure baryon number fluctuation, and found it is the most sensitive one at the same order to the LGPT critical end point. The possible reason is that the baryon number fluctuation includes both the proton and neutron's contribution. However, the electric charge fluctuation involves the isospin density,  $\rho_N - \rho_P$ . The baryon number density is always larger than the isospin density, which is associated with stronger fluctuations when there are more derivatives with respect to baryon chemical potential than that with electric chemical potential for a given order of correlations.

Additionally, comparing the results in Fig. 2-6, we can find that the rescaled higher-order correlations fluctuate more strongly near the phase transition region, while the lower-order correlations at high temperature are relatively larger than most of the higher-order ones away from the phase transition region. The similar phenomenon exist for the correlations of conserved charges in quark matter [74]. According to the fluctuations of net baryon number [55, 67], and the correlations between net baryon number and electric charge in this study, it can be seen that the fluctuations and correlations of conserved charges have similar organization structures for

nuclear and quark matter. This can be mainly attributed to that the two phase transitions belong to the same universal class and they both describe the interacting matter with temperature and chemical potential dependent fermion masses.

Since the QCD phase transition and nuclear LGPT possibly occur sequentially from high to low temperature, (even if the LGPT is not triggered) the energy dependent behaviors of fluctuations and correlations can be referenced to look for the phase transition signals of strongly interacting matter. Although the latest reported BES II high-precision data at  $7.7 - 39$  GeV does not show a drastic change of the net baryon number kurtosis, the stronger fluctuation signals possibly appear in heavy-ion experiments with collision energies lower than 7.7 GeV. Furthermore, in the hadronic interaction domain away from the phase transition region, the similar phenomenon exist for the correlations of conserved charges in quark matter [74]. According to the fluctuations of net baryon number [55, 67], and the correlations between net baryon number and electric charge in this study, it can be seen that the fluctuations and correlations of conserved charges have similar organization structures for

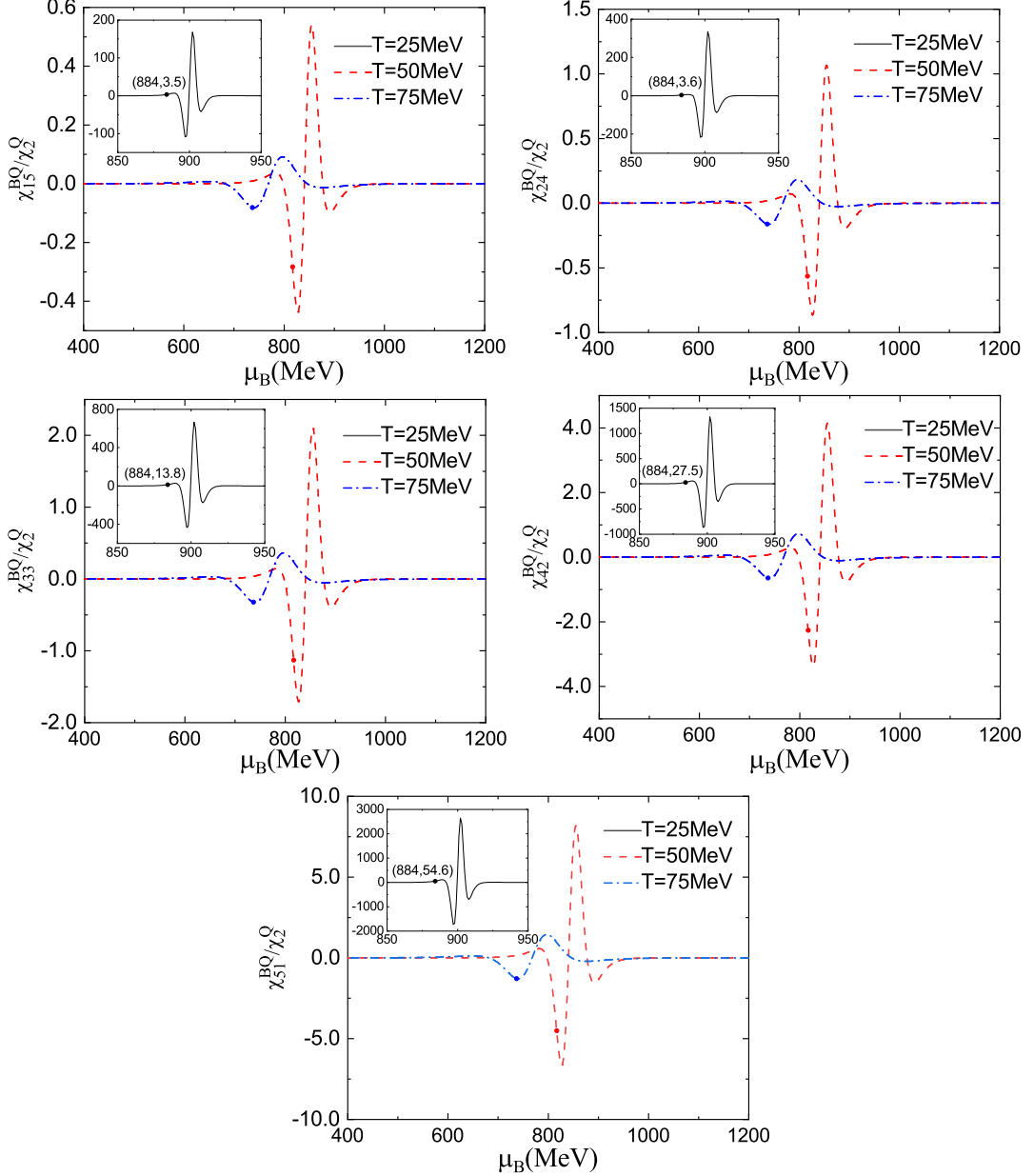


Fig. 6. Sixth order correlations between baryon number and electric charge as functions of chemical potential for different temperatures. The solid dots demonstrate the values on the chemical freeze-out line given in Fig. 1.

392

#### IV. SUMMARY

393 Fluctuations and correlations of conserved charges are  
394 sensitive probes to investigate the phase structure of  
395 strongly interacting matter. In this research, we cal-  
396 culated the correlations between net baryon number  
397 and electric charge up to sixth order caused by the  
398 hadronic interactions in nuclear matter with the non-  
399 linear Walecka model, and explored how they relate to  
400 nuclear liquid-gas phase transition.

401 The calculation indicates that the correlations be-

402 tween net baryon number and electric charge gradually  
403 become stronger from the high-temperature region to  
404 critical region of nuclear LGPT. In particular, the cor-  
405 relations are drastic at the location where the  $\sigma$  field or  
406 nucleon mass changes rapidly near the critical region.  
407 A similar behavior exists for the chiral crossover phase  
408 transition of quark matter. This is mainly attributed to  
409 the similar dynamical mass evolution and the same uni-  
410 versal class for the chiral phase transition of quark mat-  
411 ter and the liquid-gas phase transition of nuclear matter.  
412 Compared with the lower order correlations, the  
413 higher order correlations fluctuate more strongly near

414 the phase transition region, while the rescaled lower order correlations are relatively stronger than most of the higher-order ones away from the phase transition region at high temperature. At the chemical freeze-out for each temperature, the calculation shows  $\chi_{13}^{BQ}/\chi_2^Q < \chi_{22}^{BQ}/\chi_2^Q < \chi_{31}^{BQ}/\chi_2^Q$  for the fourth order correlation,  $|\chi_{14}^{BQ}/\chi_2^Q| < |\chi_{23}^{BQ}/\chi_2^Q| < |\chi_{32}^{BQ}/\chi_2^Q| < |\chi_{41}^{BQ}/\chi_2^Q|$  for the fifth order correlations, and  $|\chi_{15}^{BQ}/\chi_2^Q| < |\chi_{24}^{BQ}/\chi_2^Q| < |\chi_{33}^{BQ}/\chi_2^Q| < |\chi_{42}^{BQ}/\chi_2^Q| < |\chi_{51}^{BQ}/\chi_2^Q|$  for the sixth order correlations. In particular, the values of fifth and sixth order correlations change from negative to positive when approaching to the critical region of LGPT from the high-temperature side along the extrapolated chemical freeze-out line. With the release of more precise data in experiments below 7.7 GeV in the future, the realistic chemical freeze-out condition can be fitted and the results obtained in this research can be referred to analyze the signals of QCD phase transition and the influence of nuclear liquid-gas phase transition.

---

[1] Q.Y. Shou, Y.G. Ma, S. Zhang, et al., Properties of QCD matter: a review of selected results from ALICE experiment. *Nucl. Sci. Tech.* 35, 219 (2024). doi: [10.1007/s41365-024-01583-2](https://doi.org/10.1007/s41365-024-01583-2)

[2] Y. Aoki, G. Endrodi, Z. Fodor, et al., The order of the quantum chromodynamics transition predicted by the standard model of particle physics. *Nature* 443, 675-678 (2006). doi: [10.1038/nature05120](https://doi.org/10.1038/nature05120)

[3] A. Bazavov, H.T. Ding, P. Hegde, et al., (HotQCD Collaboration), Chiral crossover in QCD at zero and non-zero chemical potentials. *Phys. Lett. B* 795, 15 (2019). doi: [10.1016/j.physletb.2019.05.013](https://doi.org/10.1016/j.physletb.2019.05.013)

[4] S. Borsányi, Z. Fodor, S.D. Katz, et al., Freeze-Out Parameters: Lattice Meets Experiment. *Phys. Rev. Lett.* 111, 062005 (2013). doi: [10.1103/PhysRevLett.111.062005](https://doi.org/10.1103/PhysRevLett.111.062005)

[5] A. Bazavov, T. Bhattacharya, C. DeTar, et al., (HotQCD Collaboration), Equation of state in (2+1)-flavor QCD. *Phys. Rev. D* 90, 094503 (2014). doi: [10.1103/PhysRevD.90.094503](https://doi.org/10.1103/PhysRevD.90.094503)

[6] A. Bazavov, H.T. Ding, P. Hegde, et al., (HotQCD Collaboration), Skewness and kurtosis of net baryon-number distributions at small values of the baryon chemical potential. *Phys. Rev. D* 96, 074510 (2017). doi: [10.1103/PhysRevD.96.074510](https://doi.org/10.1103/PhysRevD.96.074510)

[7] S. Borsányi, Z. Fodor, C. Hoelbling, et al., Full result for the QCD equation of state with flavors. *Phys. Lett. B* 730, 99 (2014). doi: [10.1016/j.physletb.2014.01.007](https://doi.org/10.1016/j.physletb.2014.01.007)

[8] S. Borsányi, Z. Fodor, J.N. Guenther, et al., QCD Crossover at Finite Chemical Potential from Lattice Simulations. *Phys. Rev. Lett.* 125, 052001 (2020). doi: [10.1103/PhysRevLett.125.052001](https://doi.org/10.1103/PhysRevLett.125.052001)

[9] K. Fukushima, Chiral effective model with the Polyakov loop. *Phys. Lett. B* 591, 277 (2004). doi: [10.1016/j.physletb.2004.04.027](https://doi.org/10.1016/j.physletb.2004.04.027)

[10] C. Ratti, M.A. Thaler, W. Weise, Phases of QCD: Lattice thermodynamics and a field theoretical model. *Phys. Rev. D* 73, 014019 (2006). doi: [10.1103/PhysRevD.73.014019](https://doi.org/10.1103/PhysRevD.73.014019)

[11] P. Costa, M.C. Ruivo, C.A. De Sousa, et al., Phase diagram and critical properties within an effective model of QCD: the Nambu-Jona-Lasinio model coupled to the Polyakov loop. *Symmetry* 2, 1338-1374 (2010). doi: [10.3390/sym2031338](https://doi.org/10.3390/sym2031338)

[12] W.J. Fu, Z. Zhang, Y.X. Liu, 2+1 flavor Polyakov-Nambu-Jona-Lasinio model at finite temperature and nonzero chemical potential. *Phys. Rev. D* 77, 014006 (2008). doi: [10.1103/PhysRevD.77.014006](https://doi.org/10.1103/PhysRevD.77.014006)

[13] T. Sasaki, J. Takahashi, Y. Sakai, et al., Theta vacuum and entanglement interaction in the three-flavor Polyakov-loop extended Nambu-Jona-Lasinio model. *Phys. Rev. D* 85, 056009 (2012). doi: [10.1103/PhysRevD.85.056009](https://doi.org/10.1103/PhysRevD.85.056009)

[14] M. Ferreira, P. Costa, C. Providência, Deconfinement, chiral symmetry restoration and thermodynamics of (2+1)-flavor hot QCD matter in an external magnetic field. *Phys. Rev. D* 89, 036006 (2014). doi: [10.1103/PhysRevD.89.036006](https://doi.org/10.1103/PhysRevD.89.036006)

[15] Y.Q. Zhao, S. He, D.F. Hou, et al., Phase diagram of holographic thermal dense QCD matter with rotation. *J. High Energy Phys.* 04, 115 (2023). doi: [10.1007/JHEP04\(2023\)115](https://doi.org/10.1007/JHEP04(2023)115)

[16] G.Y. Shao, Z.D. Tang, X.Y. Gao, et al., Baryon number fluctuations and the phase structure in the PNJL model. *Eur. Phys. J. C* 78, 138 (2018). doi: [10.1140/epjc/s10052-018-5636-0](https://doi.org/10.1140/epjc/s10052-018-5636-0)

[17] B.J. Schaefer, M. Wagner, J. Wambach, Thermodynamics of (2+1)-flavor QCD: Confronting models with lattice studies. *Phys. Rev. D* 81, 074013 (2010). doi: [10.1103/PhysRevD.81.074013](https://doi.org/10.1103/PhysRevD.81.074013)

[18] V. Skokov, B. Friman, K. Redlich, Quark number fluctuations in the Polyakov loop-extended quark-meson model at finite baryon density. *Phys. Rev. C* 83, 054904 (2011). doi: [10.1103/PhysRevC.83.054904](https://doi.org/10.1103/PhysRevC.83.054904)

[19] L.M. Liu, J. Xu, G.X. Peng, Three-dimensional QCD phase diagram with a pion condensate in the NJL model. *Phys. Rev. D* 104, 076009 (2021). doi: [10.1103/PhysRevD.104.076009](https://doi.org/10.1103/PhysRevD.104.076009)

[20] X. Chen, D.N. Li, D.F. Hou, et al., Quarkyonic phase from quenched dynamical holographic QCD model. *J. High Energy Phys.* 2020, 73 (2020). doi: [10.1007/JHEP03\(2020\)073](https://doi.org/10.1007/JHEP03(2020)073)

[21] M. Ferreira, P. Costa, C. Providência, Presence of a critical endpoint in the QCD phase diagram from the net-baryon number fluctuations. *Phys. Rev. D* 98, 034006 (2018). doi: [10.1103/PhysRevD.98.034006](https://doi.org/10.1103/PhysRevD.98.034006)

[22] Y.H. Yang, L. He, P.C. Chu, Properties of the phase diagram from the Nambu-Jona-Lasinio model with a scalar-vector interaction. *Nucl. Sci. Tech.* 35, 166 (2024). doi: [10.1007/s41365-024-01559-2](https://doi.org/10.1007/s41365-024-01559-2)

[23] Y.D. Chen, D.N. Li, M. Huang, Inhomogeneous chiral condensation under rotation in the holographic QCD. *Phys. Rev. D* 106, 106002 (2022). doi: [10.1103/PhysRevD.106.106002](https://doi.org/10.1103/PhysRevD.106.106002)

[24] F. Gao, Y.X. Liu, QCD phase transitions using the QCD Dyson-Schwinger equation approach.

529 Nucl. Tech. (in Chinese) 46, 040015 (2024). doi: 592 [41] Y. Zhang, D.W. Zhang, X.F. Luo, Experimental study  
530 10.11889/j.02533219.2023.hjs.46.040015 593 of the QCD phase diagram in relativistic heavy-ion col-  
531 [25] S.X. Qin, L. Chang, H. Chen, et al., Phase Diagram 594 lisions. Nucl. Tech. (in Chinese) 46, 040001 (2024). doi:  
532 and Critical End Point for Strongly Interacting Quarks. 595 10.11889/j.02533219.2023.hjs.46.040001  
533 Phys. Rev. Lett. 106, 172301 (2011). doi: 10.1103/Phys- 596 [42] Q. Chen, G.L. Ma, J.H. Chen, Transport model  
534 RevLett.106.172301 597 study of conserved charge fluctuations and  
535 [26] F. Gao, J. Chen, Y.X. Liu, et al., Phase diagram 598 QCD phase transition in heavy-ion collisions.  
536 and thermal properties of strong-interaction matter. 599 Nucl. Tech. (in Chinese) 46, 040013 (2023). doi:  
537 Phys. Rev. D 93, 094019 (2016). doi: 10.1103/Phys- 600 10.11889/j.02533219.2023.hjs.46.040013  
538 RevD.93.094019 601 [43] C. Huang, Y.Y. Tan, R. Wen, et al., Reconstruction of  
539 [27] F. Gao, J.M. Pawłowski, QCD phase structure from 602 baryon number distributions. Chin. Phys. C 47, 104106  
540 functional methods. Phys. Rev. D 102, 034027 (2020). 603 (2023). doi: 10.1088/1674-1137/aceee1  
541 doi: 10.1103/PhysRevD.102.034027 604 [44] J.X. Shao, W.J. Fu, Y.X. Liu, Chemical freeze-  
542 [28] C.S. Fischer, J. Luecker, C.A. Welzbacher, Phase struc- 605 out parameters via a functional renormalization group  
543 ture of three and four flavor QCD. Phys. Rev. D 90, 606 approach. Phys. Rev. D 109, 034019 (2024). doi:  
544 034022 (2014). doi: 10.1103/PhysRevD.90.034022 607 10.1103/PhysRevD.109.034019  
545 [29] C. Shi, Y.L. Wang, Y. Jiang, et al., Locate QCD critical 608 [45] M. Marczenko, K. Redlich, C. Sasaki, Fluctuations  
546 end point in a continuum model study. J. High Energy 609 near the liquid-gas and chiral phase transitions in  
547 Phys. 1407, 014 (2014). doi: 10.1007/JHEP07(2014)014 610 hadronic matter. Phys. Rev. D 107, 054046 (2023). doi:  
548 [30] W.J. Fu, J.M. Pawłowski, F. Rennecke, QCD phase 611 10.1103/PhysRevD.107.054046  
549 structure at finite temperature and density. Phys. Rev. D 612 [46] C. Liu, X.G. Deng, Y.G. Ma, Density fluctuations in  
550 101, 054032 (2020). doi: 10.1103/PhysRevD.101.054032 613 intermediate-energy heavy-ion collisions. Nucl. Sci. Tech.  
551 [31] F. Rennecke, B.J. Schaefer, Fluctuation-induced mod- 614 33, 52 (2022). doi: 10.1007/s41365-02201040-y  
552 ifications of the phase structure in (2+1)-flavor QCD. 615 [47] P. Chomaz, M. Colonna, J. Randrup, Nuclear spin-  
553 Phys. Rev. D 96, 016009 (2017). doi: 10.1103/Phys- 616 odal fragmentation. Phys. Rep. 389, 263 (2004). doi:  
554 RevD.96.016009 617 10.1016/j.physrep.2003.09.006  
555 [32] W.J. Fu, X.F. Luo, J.M. Pawłowski, et al., Hyper- 618 [48] J. Pochodzalla, T. Mohlenkamp, T. Rubehn, et al., (AL-  
556 order baryon number fluctuations at finite tempera- 619 ADIN Collaboration), Probing the Nuclear Liquid-Gas  
557 ture and density. Phys. Rev. D 104, 094047 (2021). doi: 620 Phase Transition. Phys. Rev. Lett. 75, 1040 (1995). doi:  
558 10.1103/PhysRevD.104.094047 621 10.1103/PhysRevLett.75.1040  
559 [33] Y.G. Ma, L.G. Pang, R. Wang, et al., Phase Transition 622 [49] B. Borderie, G. Tabacaru, P. Chomaz, et al., (NDRA  
560 Study Meets Machine Learning. Chin. Phys. Lett. 40, 623 Collaboration), Evidence for Spinodal Decomposition in  
561 122101 (2023). doi: 10.1088/0256307X/40/12/122101 624 Nuclear Multifragmentation. Phys. Rev. Lett. 86, 3252  
562 [34] M.A. Stephanov, Non-Gaussian Fluctuations near the 625 (2001). doi: 10.1103/PhysRevLett.86.3252  
563 QCD Critical Point. Phys. Rev. Lett. 102, 032301 (2009). 626 [50] A.S. Botvina, I.N. Mishustin, M. Begemann-Blaich,  
564 doi: 10.1103/PhysRevLett.102.032301 627 et al., Multifragmentation of spectators in relativistic  
565 [35] M.A. Stephanov, Sign of Kurtosis near the QCD Crit- 628 heavy-ion reactions. Nucl. Phys. A 584, 737-756 (1995).  
566 ical Point. Phys. Rev. Lett. 107, 052301 (2011). doi: 629 doi: 10.1016/0375-9474(94)00621-S  
567 10.1103/PhysRevLett.107.052301 630 [51] M. D'Agostino, A.S. Botvina, M. Bruno, et al., Thermo-  
568 [36] M.M. Aggarwal, Z. Ahmed, A.V. Alakhverdyants, 631 dynamical features of multifragmentation in peripheral  
569 et al., (STAR Collaboration), Higher Moments of 632 Au + Au collisions at 35AMeV. Nucl. Phys. A 650, 329-  
570 Net Proton Multiplicity Distributions at RHIC. Phys. 633 357 (1999). doi: 10.1016/S03759474(99)00097-4  
571 Rev. Lett. 105, 022302 (2010). doi: 10.1103/Phys- 634 [52] B.K. Srivastava, R.P. Scharenberg, S. Albergo, et al.,  
572 RevLett.105.022302 635 (EOS Collaboration), Multifragmentation and the phase  
573 [37] L. Adamczyk, J.K. Adkins, G. Agakishiev, et al., 636 transition: A systematic study of the multifragmentation  
574 (STAR Collaboration), Energy Dependence of Moments 637 of 1AGeV Au, La, and Kr. Phys. Rev. C 65, 054617  
575 of Net-Proton Multiplicity Distributions at RHIC. Phys. 638 (2002). doi: 10.1103/PhysRevC.65.054617  
576 Rev. Lett. 112, 032302 (2014). doi: 10.1103/Phys- 639 [53] J.B. Elliott, L.G. Moretto, L. Phair, et al., (ISiS Col-  
577 RevLett.112.032302 640 laboration), Liquid to Vapor Phase Transition in Ex-  
578 [38] J.H. Chen, X. Dong, X.H. He, et al., Properties of the 641 cited Nuclei. Phys. Rev. Lett. 88, 042701 (2002). doi:  
579 QCD matter: review of selected results from the rel- 642 10.1103/PhysRevLett.88.042701  
580 ativistic heavy ion collider beam energy scan (RHIC 643 [54] W.B. He, G.Y. Shao, C.L. Xie, Speed of sound  
581 BES) program. Nucl. Sci. Tech. 35, 214 (2024). doi: 644 and liquid-gas phase transition in nuclear matter.  
582 10.1007/s41365-024-01591-2 645 Phys. Rev. C 107, 014903 (2023). doi: 10.1103/Phys-  
583 [39] X.F. Luo, N. Xu, Search for the QCD critical point with 646 RevC.107.014903  
584 fluctuations of conserved quantities in relativistic heavy- 647 [55] G.Y. Shao, X.Y. Gao, W.B. He, Baryon number fluctu-  
585 ion collisions at RHIC: an overview. Nucl. Sci. Tech. 28, 648 ations induced by hadronic interactions at low temper-  
586 112 (2017). doi: 10.1007/s41365-017-0257-0 649 ature and large chemical potential. Phys. Rev. D 101,  
587 [40] B.E. Aboona, J. Adam, L. Adamczyk, et al., (STAR Col- 650 074029 (2020). doi: 10.1103/PhysRevD.101.074029  
588 laboration), Measurement of Sequential  $\gamma$  Suppression in 651 [56] K. Xu, M. Huang, The baryon number fluctua-  
589 Au+Au Collisions at  $\sqrt{s_{NN}} = 200\text{GeV}$  with the STAR 652 tion  $\kappa\sigma^2$  as a probe of nuclear matter phase transi-  
590 Experiment. Phys. Rev. Lett. 130, 082301 (2023). doi: 653 tion at high baryon density. arXiv:2307.12600v1. doi:  
591 10.1103/PhysRevLett.130.112301 654 10.48550/arXiv.2307.12600

655 [57] Y.G. Ma, Application of Information Theory in Nuclear 698  
 656 Liquid Gas Phase Transition. Phys. Rev. Lett. 83, 3617 699  
 657 (1999). doi: [10.1103/PhysRevLett.83.3617](https://doi.org/10.1103/PhysRevLett.83.3617) 700

658 [58] X.G. Deng, P. Danielewicz, Y.G. Ma, et al., Impact 701  
 659 of fragment formation on shear viscosity in the nuclear 702  
 660 liquid-gas phase transition region. Phys. Rev. C 105, 703  
 661 064613 (2022). doi: [10.1103/PhysRevC.105.064613](https://doi.org/10.1103/PhysRevC.105.064613) 704

662 [59] M. Hempel, V. Dexheimer, S. Schramm, et al., Non- 705  
 663 congruence of the nuclear liquid-gas and deconfinement 706  
 664 phase transitions. Phys. Rev. C 88, 014906 (2013). doi: 707  
 665 [10.1103/PhysRevC.88.014906](https://doi.org/10.1103/PhysRevC.88.014906) 708

666 [60] A. Mukherjee, J. Steinheimer, S. Schramm, Higher-order 709  
 667 baryon number susceptibilities: Interplay between the 710  
 668 chiral and the nuclear liquid-gas transitions. Phys. Rev. 711  
 669 C 96, 025205 (2017). doi: [10.1103/PhysRevC.96.025205](https://doi.org/10.1103/PhysRevC.96.025205) 712

670 [61] J. Xu, L.W. Chen, C.M. Ko, et al., Shear viscosity 713  
 671 of neutron-rich nucleonic matter near its liquid-gas 714  
 672 phase transition. Phys. Lett. B 727, 244 (2013). doi: 715  
 673 [10.1016/j.physletb.2013.10.051](https://doi.org/10.1016/j.physletb.2013.10.051) 716

674 [62] O. Savchuk, V. Vovchenko, R.V. Poberezhnyuk, et al., 717  
 675 Traces of the nuclear liquid-gas phase transition in the 718  
 676 analytic properties of hot QCD. Phys. Rev. C 101, 719  
 677 035205 (2020). doi: [10.1103/PhysRevC.101.035205](https://doi.org/10.1103/PhysRevC.101.035205) 720

678 [63] R. Wang, Y.G. Ma, R. Wada, et al., Nuclear liquid- 721  
 679 gas phase transition with machine learning. Phys. 722  
 680 Rev. Res. 2, 043202 (2020). doi: [10.1103/PhysRevRes.2.043202](https://doi.org/10.1103/PhysRevRes.2.043202) 723

681 [64] R.V. Poberezhnyuk, V. Vovchenko, A. Motornenko, et 725  
 682 al., Chemical freeze-out conditions and fluctuations of 726  
 683 conserved charges in heavy-ion collisions within a quan- 727  
 684 tum van der Waals model. Phys. Rev. C 100, 054904 728  
 685 (2019). doi: [10.1103/PhysRevC.100.054904](https://doi.org/10.1103/PhysRevC.100.054904) 729

686 [65] V. Vovchenko, M.I. Gorenstein, H. Stöecker, van der 730  
 687 Waals Interactions in Hadron Resonance Gas: From 731  
 688 Nuclear Matter to Lattice QCD. Phys. Rev. Lett. 118, 732  
 689 182301 (2017). doi: [10.1103/PhysRevLett.118.182301](https://doi.org/10.1103/PhysRevLett.118.182301) 733

690 [66] R.V. Poberezhnyuk, O. Savchuk, M.I. Gorenstein, et 734  
 691 al., Higher order conserved charge fluctuations inside 735  
 692 the mixed phase. Phys. Rev. C 103, 024912 (2021). doi: 736  
 693 [10.1103/PhysRevC.103.024912](https://doi.org/10.1103/PhysRevC.103.024912) 737

694 [67] X.R. Yang, G.Y. Shao, W.B. He, Fifth- and sixth-order 738  
 695 low temperature. Phys. Rev. C 109, 014908 (2024). doi: 740  
 696 [10.1103/PhysRevC.109.014908](https://doi.org/10.1103/PhysRevC.109.014908) 741

[68] M. Bluhm, A. Kalweit, M. Nahrgang, et al., Dynamics of critical fluctuations: Theory - phenomenology - heavy-ion collisions. Nucl. Phys. A 1003 (2020) 122016. doi: [10.1016/j.nuclphysa.2020.122016](https://doi.org/10.1016/j.nuclphysa.2020.122016)

[69] R. Bellwied, S. Borsányi, Z. Fodor, et al., Fluctuations and correlations in high temperature QCD. Phys. Rev. D 92, 114505 (2015). doi: [10.1103/PhysRevD.92.114505](https://doi.org/10.1103/PhysRevD.92.114505)

[70] R. Wen, W.J. Fu, Correlations of conserved charges and QCD phase structure. Chin. Phys. C 45, 044112 (2021). doi: [10.1088/1674-1137/abe199](https://doi.org/10.1088/1674-1137/abe199)

[71] H.T. Ding, S. Mukherjee, H. Ohno, et al., Diagonal and off-diagonal quark number susceptibilities at high temperatures. Phys. Rev. D 92, 074043 (2015). doi: [10.1103/PhysRevD.92.074043](https://doi.org/10.1103/PhysRevD.92.074043)

[72] S. Borsányi, Z. Fodor, J.N. Guenther, et al., Higher order fluctuations and correlations of conserved charges from lattice QCD. J. High Energy Phys. 10, 205 (2018). doi: [10.1007/JHEP10\(2018\)205](https://doi.org/10.1007/JHEP10(2018)205)

[73] R. Bellwied, S. Borsányi, Z. Fodor, et al., Off-diagonal correlators of conserved charges from lattice QCD and how to relate them to experiment. Phys. Rev. D 101, 034506 (2020). doi: [10.1103/PhysRevD.101.034506](https://doi.org/10.1103/PhysRevD.101.034506)

[74] W.J. Fu, Y.L. Wu, Fluctuations and correlations of conserved charges near the QCD critical point. Phys. Rev. D 82, 074013 (2010). doi: [10.1103/PhysRevD.82.074013](https://doi.org/10.1103/PhysRevD.82.074013)

[75] A. Bhattacharyya, P. Deb, A. Lahiri, et al., Correlation between conserved charges in Polyakov–Nambu–Jona-Lasinio model with multiquark interactions. Phys. Rev. D 83, 014011 (2011). doi: [10.1103/PhysRevD.83.014011](https://doi.org/10.1103/PhysRevD.83.014011)

[76] H.T. Ding, F. Karsch, S. Mukherjee, Thermodynamics of strong-interaction matter from lattice QCD. Int. J. Mod. Phys. E 24, 530007 (2015). doi: [10.1142/S0218301315300076](https://doi.org/10.1142/S0218301315300076)

[77] K. Fukushima, Hadron resonance gas and mean-field nuclear matter for baryon number fluctuations. Phys. Rev. C 91, 044910 (2015). doi: [10.1103/PhysRevC.91.044910](https://doi.org/10.1103/PhysRevC.91.044910)

[78] N.K. Glendenning, COMPACT STARS, Nuclear Physics, Particle Physics, and General Relativity 2nd edn. (Springer, New York, 2000), pp.189

[79] J. Cleymans, H. Oeschler, K. Redlich, et al., Comparison of chemical freeze-out criteria in heavy-ion collisions. Phys. Rev. C 73, 034905 (2006). doi: [10.1103/PhysRevC.73.034905](https://doi.org/10.1103/PhysRevC.73.034905)